Journal of Anatomy

J. Anat. (2011) **218**, pp59–74 doi: 10.1111/j.1469-7580.2010.01319.x

The impact of bone and suture material properties on mandibular function in *Alligator mississippiensis*: testing theoretical phenotypes with finite element analysis

David A. Reed,[1] Laura B. Porro,[1] Jose Iriarte-Diaz,[1] Justin B. Lemberg,[1] Casey M. Holliday,[2] Fred Anapol[3] and Callum F. Ross[1]

[1]*Department of Organismal Biology and Anatomy, University of Chicago, Chicago, IL, USA*
[2]*Department of Pathology and Anatomical Sciences, University of Missouri School of Medicine, Columbia, MO, USA*
[3]*Department of Anthropology, University of Wisconsin Milwaukee, Milwaukee, WI, USA*

Abstract

The functional effects of bone and suture stiffness were considered here using finite element models representing three different theoretical phenotypes of an *Alligator mississippiensis* mandible. The models were loaded using force estimates derived from muscle architecture in dissected specimens, constrained at the 18th and 19th teeth in the upper jaw and 19th tooth of the lower jaw, as well as at the quadrate-articular joint. Stiffness was varied systematically in each theoretical phenotype. The three theoretical phenotypes included: (i) linear elastic isotropic bone of varying stiffness and no sutures; (ii) linear elastic orthotropic bone of varying stiffness with no sutures; and (iii) linear elastic isotropic bone of a constant stiffness with varying suture stiffness. Variation in the isotropic material properties of bone primarily resulted in changes in the magnitude of principal strain. By comparison, variation in the orthotropic material properties of bone and isotropic material properties of sutures resulted in: a greater number of bricks becoming either more compressive or more tensile, changing between being either dominantly compressive or tensile, and having larger changes in the orientation of maximum principal strain. These data indicate that variation in these model properties resulted in changes to the strain regime of the model, highlighting the importance of using biologically verified material properties when modeling vertebrate bones. When bones were compared within each set, the response of each to changing material properties varied. In two of the 12 bones in the mandible, varied material properties within sutures resulted in a decrease in the magnitude of principal strain in bricks adjacent to the bone/suture interface and decreases in stored elastic energy. The varied response of the mandibular bones to changes in suture stiffness highlights the importance of defining the appropriate functional unit when addressing relationships of performance and morphology.

Key words biomechanics; crocodilians; feeding.

Introduction

The relationship of bone morphology to the strain resulting from external loading is central to the understanding of both the evolution (Hylander, 1984; Rubin & Lanyon, 1984; Biewener & Taylor, 1986; Hylander et al. 1991; Ross, 2001) and development (Moss et al. 1972; Carter & Beaupre, 2001; Nowlan et al. 2007, 2008) of skeletal phenotypes. The overall strain environment, encompassed by concepts of strain gradients and overall deformation regimes, may be more informative than localized strain measurements for understanding the functional consequences of loading across complex morphologies (Hylander, 1984; Hylander & Johnson, 1994; Rafferty & Herring, 1999; Ravosa et al. 2000; Ross, 2001; Ross & Metzger, 2004; Metzger et al. 2005). Strain gradients and global deformation regimes can be inferred from measurements from multiple strain gage sites (Hylander, 1984; Ross, 2001; Ross & Metzger, 2004; Metzger et al. 2005), or these patterns can be calculated *in silico* using finite element modeling (Richmond et al. 2005; Ross, 2005). Finite element analysis (FEA) has the benefit of allowing strain and deformation regimes to be characterized in theoretical scenarios that would be difficult, if not impossible,

Correspondence
David A. Reed, Department of Organismal Biology and Anatomy, University of Chicago, 1027 East 57th Street, Chicago, IL 60637, USA.
F: 773 702 0037; E: dreed@uchicago.edu

Accepted for publication *15 October 2010*
Article published online *22 November 2010*

to test *in vivo*. For example, the material properties of the bone and suture in the model can be easily manipulated and compared. Several studies have used this technique to compare *in vivo* strain measurements to local behavior of a model in an effort to determine the boundary conditions and material properties most representative of the *in vivo* data, i.e. model validation through sensitivity analysis (Sellers & Crompton, 2004; Wang et al. 2004; Marinescu et al. 2005; Ross et al. 2005; Strait et al. 2005; Kupczik et al. 2007). Validated models are essential for development of biologically realistic models.

Robust comparisons of strain and deformation regimes in theoretical finite element models (FEMs) can also yield meaningful biological insights. One of the most important foci of such theoretical analyses is the influence of bone material properties on strain and deformation regimes. Bone material properties vary both within individuals (Yamada & Evans, 1970; Papadimitriou et al. 1996; Peterson & Dechow, 2002; Schwartz-Dabney & Dechow, 2002; Wang & Dechow, 2004) and across amniotes (Currey, 1987, 2002; Erickson et al. 2002), and have in some cases been found to be correlated with their functional environment (Currey, 1979, 1999). While the precise functional consequences of variability in bone material properties can be investigated *in vivo*, the complexity of organisms makes it difficult to control other variables that might confound the results. Theoretical modeling of material properties in a single morphology using FEA makes it possible to control all aspects of the functional complex, allowing the influence of material properties to be isolated.

As part of a larger study of *in vivo* bone strain, material properties, geometry and developmental plasticity in the *Alligator* mandible (K.A. Metzger, C.F. Ross, L.B. Porro, unpublished communication; L.B. Porro, D.A. Reed, J. Iriarte-Diaz, J. Lemberg, C. Holliday, F. Anapol, CF. Ross, unpublished communication; Zapata et al. 2010), this paper investigates the effects of bone orthotropy and suture stiffness on the strain and deformation regimes of the mandible of *Alligator mississippiensis*. Strain and deformation regimes were compared across 30 FEMs representing three sets, each consisting of 10 trials, across which elastic modulus was incrementally varied. In the first set, the mandible was modeled as linear elastic isotropic bone with no sutures (i.e. sutures were given the same material properties as bone), and the stiffness of all the bone material was varied. This generated a baseline against which the other two sets could be compared. In the second set, the mandible was modeled as linear elastic orthotropic bone with no sutures, and the stiffness of the bone material was varied only along the rostrocaudal axis. The *Alligator* mandible has been shown to be transversely anisotropic (orthotropic), with the maximal axis of stiffness along the rostrocaudal axis (Zapata et al. 2010), and our experimental design was aimed at quantifying these effects. In the third set, the mandible was modeled with a constant linear elastic isotropic stiffness in the bones and varied linear elastic isotropic material properties in the sutures. The impact of suture stiffness on strain and deformation regimes in the vertebrate mandible and crania is of interest because principal strain magnitudes over sutures have been found to be considerably higher than in the surrounding bone (Hubbard, 1971; Behrents et al. 1978; Oudhof & Doorenmaalen, 1983; Smith & Hylander, 1985; Herring & Mucci, 1991; Herring, 1993; Jaslow & Biewener, 1995; Persson, 1995; Rafferty & Herring, 1999; Herring & Teng, 2000; Sun et al. 2002, 2004; Rafferty et al. 2003; Popowics & Herring, 2007), leading many to suggest that sutures act to store elastic energy and thereby decrease stress and strain in the surrounding bones (Pritchard et al. 1956; Buckland-Wright, 1972, 1978; Berhents et al. 1978; Jaslow, 1990; Herring & Teng, 2000; Rafferty et al. 2003; Rayfield, 2005). This hypothesis was examined by varying suture stiffness within ranges reported in the literature on vertebrates (Radhakrishnan & Mao, 2004; Kupczik et al. 2007), and assessing the functional consequence of localized alterations in material properties on patterns of the strain and deformation in the mandible.

The predicted behavior of the model in these three sets of trials can be derived from continuum mechanics: the deflection of a solid body is inversely proportional to a material's stiffness at a given load, so it is expected that decreasing stiffness at a given load will result in a higher magnitude of deflection. The trajectory of the deformation in the orthotropic condition is expected to diverge from that of the isotropic condition as defined by the constitutive equations of Hooke's law in orthotropic materials, stating that the tri-axial state of a given elastic modulus will impact the associated tri-axial components of strain at a given stress (Hibbeler, 2004). A similar prediction can be made when a linear elastic isotropic material of differing properties is distributed heterogeneously throughout the model, as with the suture condition, although there are no constitutive equations with which to make predictions.

Thus, we hypothesized that: (H_1) decreasing the stiffness of *isotropic* bone in a mandible without sutures would result in an increase in the magnitude of maximum and minimum principal strain with little change in the orientation of maximum principal strain or the direction of nodal displacement; (H_2) decreasing the stiffness of *orthotropic* bone in a mandible without sutures would also result in an increase in the magnitude of maximum and minimum principal strain, but in association with a greater impact on the orientation of maximum principal strain and the direction of nodal displacement compared with the isotropic condition; and (H_3) decreasing the stiffness of sutures in a mandible with isotropic bones would result in either no changes or decreases in the magnitude of maximum and minimum principal strain in the bones, along with greater variation in the orientation of maximum principal strain and direction of nodal displacement compared with the isotropic condition.

Materials and methods

Construction of the FEM

The skull of an adult *Alligator mississippiensis* with a basal skull length of 16 cm was scanned using a GE Lightspeed 16 CT scanner at 100 kV and 70 mA, with a slice thickness of 0.31 mm and a resolution of 0.254 mm per pixel. The scan was processed and segmented in Amira (v5.2.2, Visage Imaging, Berlin, Germany, http://www.visageimaging.com). Segmented structures included all mandibular bones, sutures, periodontium and teeth. The segmented model was imported into Strand7 (v2.4.1, Strand7, Sydney, Australia, http://www.strand7.com) and meshed, resulting in 641 085 elements representing the mandible and 360 399 elements representing the cranium. Elements were constructed as linear tetrahedrons, consisting of four nodes at the apices of the tetrahedra. A global coordinate system was defined in the segmented model and imported into Strand7 (Fig. 1).

The model was loaded using force estimates derived from muscle architecture. Muscle origins and insertions were mapped onto the meshed FEM from dissected specimens of similar skull length, and largely follow Holliday & Witmer (2007) and Holliday (2009). Muscle fiber lengths and pinnation angles from up to six fibers were calculated and averaged within each muscle. Normalized fiber length was calculated correcting for sarcomere contraction using an optimum sarcomere length of 2.5 μm (Anapol & Barry, 1996). Reduced physiological cross-sectional area (RPCA) was then calculated using the equation:

$$RPCA = \frac{M_{\text{muscle}}\text{Cos}\theta}{L_f 1.0564},$$

where M_{muscle} is muscle weight, θ is pinnation angle, L_f is normalized fiber length, and 1.0564 is the specific gravity of the muscle (Murphy & Beardsley, 1974). Maximum possible force production ($F_{p\ max}$) was calculated using the equation:

$$F_{p\ max} = \text{RPCA} \times 30\ \text{N cm}^{-2}$$

Muscle forces at a 30 ° gape (F_{p30}) were calculated following the methods outlined in Porro et al. (unpublished communication), and applied to the model using Boneload, a Microsoft Visual Basic program authored by Grosse et al. (2007). This program accounts for the mechanics of muscle wrapping around curved surfaces in the model. The model was fixed in all six degrees of freedom at the toothrow using the 18th and 19th tooth on the upper jaw and the 19th tooth on the lower jaw. Tooth restraints were chosen based on bite points from *in vivo* transducer data (Metzger et al., unpublished communication; Porro et al., unpublished communication). Constraints at the quadrate–articular joint were modeled as a ring of nodes around the periphery of the joint surface (on both the quadrate and articular), preventing disarticulation of the joint along the *x*, *y* and *z* axes, thus acting as the ligaments that bind the joint capsule. The nodes within this ring were constrained against compression along the *y* axis, thus preventing the joint surfaces from moving towards each other.

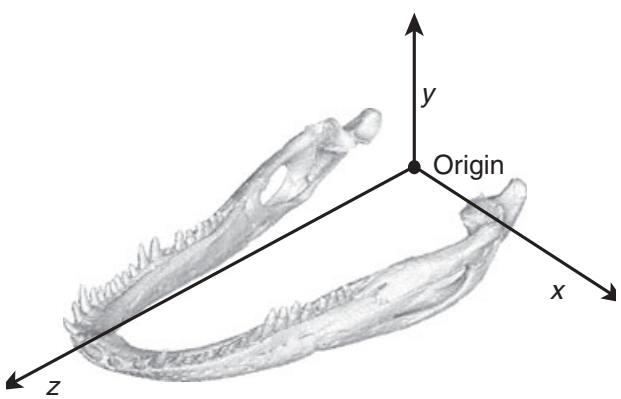

Fig. 1 The global coordinate system of the FEM: *x*- and *y*-axes define the coronal plane; the *y*- and *z*-axes define the sagittal plane; and the *z*- and *x*-axes define the transverse plane. Positive *x* is to the animal's left, positive *y* is dorsal, and positive *z* is rostral.

The model boundary conditions defined by muscle forces and constraints were held constant for all analyses. Variation in the displacement and strain output of the model was generated by varying bone and suture material properties across 10 separate trials in each of three sets. The first set modeled a mandible with isotropic bone and no sutures. The elastic modulus of the bone in this set was decreased from 20 to 9.58 GPa, a range representative of the extremes reported in Zapata et al. (2010), through 10 trials, with each incremental decrease in the set being equal. Bricks representing suture locations were included in the model but given the material properties of the surrounding bone. The second set represented a model with orthotropic bone and no sutures. The bone had a constant elastic modulus of 9 GPa in dorsoventral and mediolateral axes, and an elastic modulus along the rostrocaudal axis decreasing from 20 to 9.58 GPa through 10 trials, with each incremental decrease in the set being equal. Just as in the isotropic condition of set 1, suture locations were given the material properties of the surrounding bone. The third set represented a model with isotropic bone having a constant elastic modulus of 20 GPa, and with sutures decreasing in stiffness from 12.1 GPa to 640 MPa through the 10 trials, with each incremental decrease in the set being equal.

Assessing global strain patterns with stored elastic energy

Stored elastic energy (*U*), or total strain energy, is a measure of the work expended deforming a structure (Dumont et al. 2009). To assess the impact of sutures on deformation within the bones, *U* was exported from Strand7 for each of the 12 mandibular bones, with nodes/bricks representing sutures excluded from the calculation of stored elastic energy. To assess the impact of sutures on the global behavior of the model, *U* was exported from Strand7 for all bones in the mandible, excluding the bricks representing suture locations, and for all bricks in the model including those representing suture locations.

Characterizing the impact of material properties on stored elastic energy with an analysis of variation of the strain

Strain tensors from Strand7 representing each of the 30 trials were exported to Matlab (version 7.7.0.471), and the orientation and magnitude of maximum and minimum principal strain were calculated. A subset of 250 bricks was randomly selected from each bone and used for the analysis of the strain data. Brick numbers were identical in all 30 trials and the same brick

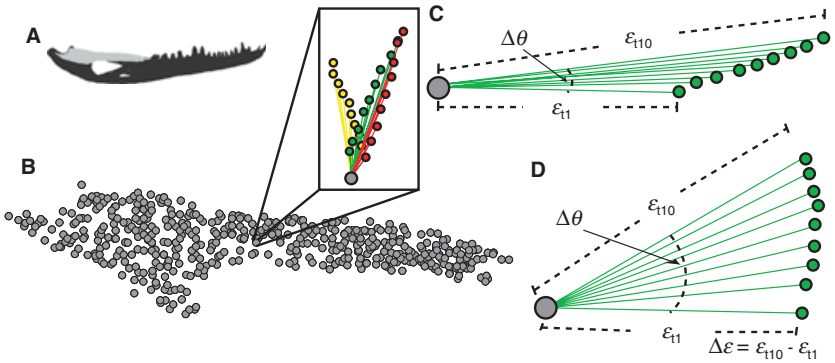

Fig. 2 Diagram describing how variation in strain is quantified. (a) Diagram of the entire working side mandible with the surangular in light gray. (b) Sub-sampled bricks from the working side surangular. The box shows the vectors (lines) and their tips (colored circles) from a single brick (gray circle) representing the magnitude and orientation of maximum principal strain from each of the 30 trials. The three colors in the box correspond to the three sets. (c and d) Diagrams showing 10 vectors (green circles and lines) describing the magnitude and orientation of maximum principal strain at a single brick (gray circle) in set 1. The stiffest trial in this set is defined as ε_{t1} and the least stiff trial in this set is defined as ε_{t10}. The variable $\Delta\theta$ describes the three-dimensional angle formed by the orientation of ε_{t1} relative to ε_{t10}. The variable $\Delta\varepsilon$ describes the difference in the magnitude of maximum principal strain between ε_{t10} and ε_{t1}. (c) A scenario in which there is very little change in $\Delta\theta$ but large changes in $\Delta\varepsilon$. (d) A scenario in which there are large changes in $\Delta\theta$ but small changes in $\Delta\varepsilon$.

list was used for all analyses of the strain data. From the sub-sampled strain data, the extremes of the differences in both the orientation and magnitude of maximum and minimum principal strain were observed at the stiffest and least stiff trials (Fig. 2). The difference in magnitude of maximum principal strain ($\Delta\varepsilon_1$) and minimum principal strain ($\Delta\varepsilon_3$) was calculated at each sub-sampled brick with the equation:

$$\Delta\varepsilon = \varepsilon_{t10} - \varepsilon_{t1},$$

with ε_{t10} corresponding to the magnitude of principal strain in the least stiff condition (trial 10), and ε_{t1} corresponding to the magnitude of maximum principal strain in the stiffest condition (trial 1). The resulting data matrix of $\Delta\varepsilon$ consisted of three points, corresponding to each of the three sets for each of the sub-sampled bricks, with each point representing the range of maximum and minimum principal strain magnitude between the least stiff and stiffest trial in each set. $\Delta\varepsilon$ in each set was further divided into four groups for each bone: those bricks that increase in their magnitude of both ε_1 and ε_3; those bricks that decrease in their magnitude of both ε_1 and ε_3; those bricks that increase in ε_1 and decrease in ε_3; and those bricks that decrease in ε_1 and increase in ε_3. The number of bricks in each group was calculated.

To determine the dominant component of principal strain, the ratio of ε_1 and ε_3 was calculated for each sub-sampled brick in each loading case. The number of bricks that switched from values of $\varepsilon_1/|\varepsilon_3| > 1$ (indicating tension) to values of $\varepsilon_1/|\varepsilon_3| < 1$ (indicating compression) between the stiffest and least stiff trials in each set was calculated. Conversely, the number of bricks switching from compression to tension was also calculated. The net number of bricks changing in their dominant loading regime between the stiffest and least stiff conditions was then calculated and expressed as a percentage of all sub-sampled bricks. Negative values indicate that the bone became more compressive in each set and positive values indicate that the bone became more tensile in each set.

To assess the extent to which the orientation of the principal strains were changing, the difference in the orientation of maximum principal strain (θ) at each brick was calculated by finding the angle between the two three-dimensional vectors describing the orientation of the least stiff and stiffest trials. $\Delta\theta$ was calculated for each of the sub-sampled bricks for each of the three sets. A value of 0 radians indicated no change in the orientation of maximum principal strain as stiffness decreased, and 1.57 radians indicates the largest possible difference in the orientation of maximum principal strain as stiffness decreased.

Characterizing the impact of material properties on the direction of nodal displacement with a multivariate analysis

Displacement data from each of the 12 bones of the mandible were exported from Strand7 and loaded in Matlab (version 7.7.0.471). A subset of 500 nodes was randomly selected from each bone and used for the analysis of the displacement data. Node numbers were identical in all 30 trials, and the same node list was used for all analyses of the displacement data. At each sub-sampled node, there were 30 positions representing variation in nodal displacement associated with the 10 trials in each of the three sets (Fig. 3). A principal component analysis (PCA) was performed on the displacement data, pooled by the 10 trials defining each set. The scores and coefficients from the PCA were used to calculate an orthogonal (total least squares) regression for each node at each set. The total least squares regression resulted in vectors describing the primary axis of variation (PC1) through the 10 displaced positions at each node for each set. A unit vector was calculated, and the three scalar components of the 500 unit vectors in each set, corresponding to the three axes in the global coordinate system, were binned by axes. The mean and standard deviation from the resulting 500 scalar values of '*x*', '*y*' and '*z*' in each set were calculated. These values therefore reflect the direction of the primary axis of variation described by PC1 resulting from changes in model material properties as defined by each of the three sets. The length of this vector was also calculated, reflecting the magnitude of the variation in nodal displacement described by PC1.

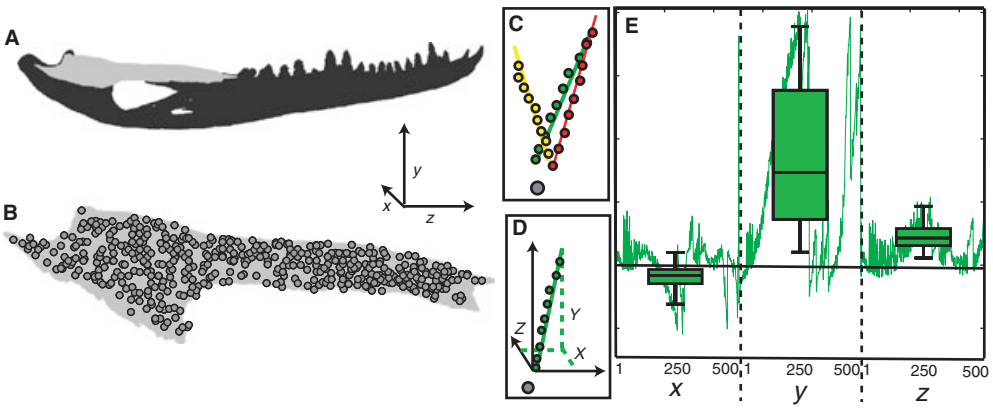

Fig. 3 Diagram describing how variation in the displacement was calculated. (a) Diagram of the entire working side mandible with the working side surangular in light gray. The global coordinate system is defined in the lower right portion of this image. (b) Diagram of the working side surangular with all 500 sub-sampled nodes superimposed over the image. (c) Diagram showing 30 displaced positions of a single node (colored circles) relative to the undeformed position of that node (gray circle). The three colors in this plot correspond to the three sets, each of 10 trials. The colored lines represent the vectors describing principal component one from the total least squares regression on the data in each set. (d) Diagram showing a point cloud representing the 10 displaced positions of a single set (green circles) relative to the undisplaced position of the node (gray circle). The solid green line represents the vector describing principal component one from the total least squares regression on the data in this set. The black arrows represent the orientation of the global coordinate system. The green dotted lines show how the vector can be described by the axes of the global coordinate system. (e) Diagram of a line plot (green line) representing the contribution of each axis to the unit vector describing the orientation of the total least squares vector from principal component one at each of the 500 sub-sampled nodes. The box plots superimposed over the line plot represent the mean and standard deviation associated with each axis.

Results

Assessing global strain patterns with stored elastic energy

In set 1, *U* increases in all bones as the stiffness decreases isotropically from 20 to 9.58 GPa (Table 1; Fig. 4). Similarly in set 2, *U* increases as bone stiffness along the *z*-axis decreases from 20 to 9.58 GPa, and stiffness along the mediolateral and dorsoventral axes is held constant at 9 GPa. As bone stiffness is decreased in set 2, *U* approaches the values in the isotropic condition of set 1. This is expected as set 2 becomes increasingly more isotropic as stiffness is decreased, i.e. the rostrocaudal axis approaches a stiffness of 9.58 GPa (Fig. 4). In set 3, it was predicted that if suture stiffness decreases isotropically from 12.1 GPa to 640 MPa, *U* in the bones with a constant isotropic stiffness of 20 GPa would either remain unchanged or decrease as more of the applied force is converted to stored elastic strain energy in the sutures. However, *U* changed differently in different bones. In the balancing and working side surangular and the balancing side coronoid, *U* decreased, as predicted. However, contrary to our predictions, decreases in suture stiffness were accompanied by increases in *U* in the balancing and working side dentaries, angulars, articulars, splenials, and in the working side coronoid (Table 1).

In sum, these data reveal that changes in strain energy with changes in material properties can be complex, depending on the orientations and locations of the changes in material properties and possibly on model geometry. This suggests that changes in material properties may result in changes in internal deformation and strain regimes. This possibility was assessed by evaluating the effect of material properties on the magnitude and orientation of maximum and minimum principal strains.

The impact of material properties on relative magnitudes and orientations of principal strains

The impact of material properties on the magnitude of principal strain was assessed by calculating the difference in magnitude between the least stiff and stiffest trials in each set for both maximum ($\Delta\varepsilon_1$) and minimum ($\Delta\varepsilon_3$) principal strain. Maximum principal strains (i.e. tension) are positive values, thus increases in magnitude are registered as positive numbers. Minimum principal strains (i.e. compression) are negative values, thus increases in magnitude are registered as negative numbers. However, in what follows we refer to positive values of $\Delta\varepsilon_1$ and negative values of $\Delta\varepsilon_3$ as 'increases' in the magnitude of each principal strain component, with the converse being true of 'decreases' in the magnitude.

In set 1, as the stiffness of isotropic bone decreased, nearly all sampled bricks in all bones displayed increases in the magnitude of both ε_1 and ε_3. In set 2, as stiffness was decreased along the *z*-axis, the majority of bricks also increased in their magnitude of both ε_1 and ε_3; however, compared with set 1, a greater number of bricks decreased in either one or both of the components of principal strain. Similarly in set 3, as suture stiffness was decreased, the

Table 1 Differences in stored elastic energy [$\times 10^{-3}$ (J mm^{-3})] between least stiff and stiffest trials in each set.

	Set 1	Set 2	Set 3
Balancing side			
Angular	0.4904 (0.6540, 1.1444)	0.3309 (0.8443, 1.1753)	0.0628 (0.6659, 0.7286)
Articular	0.7010 (0.9656, 1.6666)	0.1673 (1.5750, 1.7422)	0.3282 (1.0133, 1.3414)
Coronoid	0.0601 (0.0765, 0.1366)	0.0506 (0.0903, 0.1409)	**−0.0030** (0.0773, 0.0744)
Dentary	0.1636 (0.1973, 0.3609)	0.0745 (0.3055, 0.3800)	0.0584 (0.2000, 0.2584)
Splenial	0.0906 (0.0793, 0.1699)	0.0604 (0.1172, 0.1775)	0.0116 (0.0806, 0.0921)
Surangular	0.5351 (0.7977, 1.3329)	0.2781 (1.1009, 1.3790)	**−0.0526** (0.7979, 0.7453)
All bones	2.0410 (2.7703, 4.8112)	0.9616 (4.0332, 4.9948)	0.4053 (2.8350, 3.2402)
All bones and sutures	2.2001 (3.0056, 5.2057)	1.0402 (4.3617, 5.4019)	0.8366 (3.0715, 3.9081)
Working side			
Angular	0.2331 (0.4264, 0.6595)	0.1493 (0.525, 0.6743)	0.0200 (0.4340, 0.4540)
Articular	0.4230 (0.8013, 1.2243)	0.0932 (1.1795, 1.2727)	0.1721 (0.8339, 1.0060)
Coronoid	0.0090 (0.0243, 0.0333)	0.0003 (0.0338, 0.0341)	0.0001 (0.0247, 0.0249)
Dentary	0.1978 (0.1375, 0.3354)	0.1381 (0.2281, 0.3661)	0.0439 (0.1428, 0.1867)
Splenial	0.0611 (0.0308, 0.0918)	0.0443 (0.0569, 0.1011)	0.0128 (0.0328, 0.0456)
Surangular	0.1226 (0.4105, 0.5331)	0.0421 (0.5039, 0.5459)	**−0.0979** (0.4051, 0.3071)
All bones	1.0464 (1.8307, 2.8773)	0.4671 (2.5371, 2.9943)	0.1509 (1.8734, 2.0243)
All bones and sutures	1.1208 (1.9914, 3.1122)	0.5034 (2.7340, 3.2374)	0.3952 (2.0294, 2.4246)

Parentheses contain the values of stored elastic energy from the stiffest and least stiff trials for each bone in each set. Values reflect the difference in stored elastic energy between the least stiff and stiffest trials. Note that all differences are positive, with the exception of the working and balancing side surangulars and the balancing side coronoid in set 3. This negative value is not seen when all bones are considered together. Also note that the difference in stored elastic energy between the least stiff and stiffest trials is higher when sutures are included in the calculation for all sets, but most dramatically in set 3.

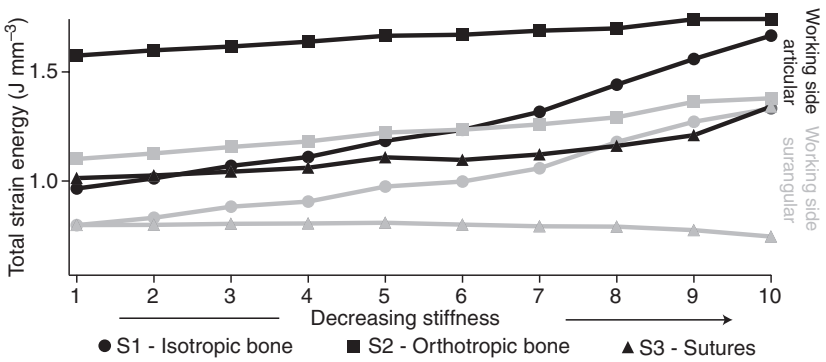

Fig. 4 Plot showing changes in stored elastic energy (values reported $\times 10^{-3}$), plotted on the '*y*' axis, with decreases in stiffness in the 10 trials in each set, plotted along the '*x*' axis. Set 1, isotropic bone with no sutures, is represented by circles; set 2, orthotropic bone with no sutures, is represented with squares; and set 3, isotropic bone with sutures, is represented by triangles. The stiffest trial is to the left and the least stiff is to the right. Results for two bones are plotted here, the working side articular in black and the working side surangular in gray. In the working side articular, stored elastic energy in all sets increases as stiffness decreases. Stored elastic energy is smaller in the isotropic condition (circles) than it is in the orthotropic condition (squares); however, the rate at which stored elastic energy increases is smaller in the orthotropic condition such that as it approaches isotropy the two values converge. Stored elastic energy in set 3 (triangles) is smaller in all trials compared with the isotropic (circles) and orthotropic (squares) conditions. This trend and relationship among the sets is representative of all bones in the mandible, with the exception of the working and balancing side surangulars (summarized in Table 1). For the working side surangular plotted here, stored elastic energy in sets one and two increases as stiffness decreases. For set 3, stored elastic energy decreases as suture stiffness decreases.

majority of bricks in most bones increased their magnitude of ε_1 and ε_3; however, compared with set 1 a greater number of bricks decreased in either one or both of the components of principal strain. Importantly, however, in set 3 the majority of bricks in the balancing side surangular and working side coronoid *decreased* in the magnitudes of both ε_1 and ε_3 as suture stiffness decreased (Table 2). For these two bones, decreasing values of *U* are accompanied by decreases in the magnitude of principal strain as suture stiffness decreases.

To assess whether the dominant component of principal strain changed, the ratio of $\varepsilon_1/|\varepsilon_3|$ was calculated. Changes in the dominant loading regime were identified in all sets and bones. Between sets, the largest number

Table 2 Number of bricks that increase and decrease their magnitude of maximum and minimum principal strain.

Bone	Set 1				Set 2				Set 3			
	(+) ε_1 & ε_3 (%)	(−) ε_1 & ε_3 (%)	(+) ε_1 (−) ε_3 (%)	(−) ε_1 (+) ε_3 (%)	(+) ε_1 & ε_3 (%)	(−) ε_1 & ε_3 (%)	(+) ε_1 (−) ε_3 (%)	(−) ε_1 (+) ε_3 (%)	(+) ε_1 & ε_3 (%)	(−) ε_1 & ε_3 (%)	(+) ε_1 (−) ε_3 (%)	(−) ε_1 (+) ε_3 (%)
Balancing side												
Angular	248 (99.2)	0 (0.0)	0 (0.0)	2 (0.8)	194 (77.6)	11 (4.4)	13 (5.2)	32 (12.8)	149 (59.6)	47 (18.8)	21 (8.4)	33 (13.2)
Articular	246 (98.4)	0 (0.0)	1 (0.4)	1 (0.4)	145 (58.0)	27 (10.8)	30 (12.0)	46 (18.4)	201 (80.4)	8 (3.2)	20 (8.0)	19 (7.6)
Coronoid	250 (100)	0 (0.0)	0 (0.0)	0 (0.0)	219 (87.6)	0 (0.0)	30 (12.0)	1 (0.4)	61 (24.4)	121 (48.4)	40 (16.0)	28 (11.2)
Dentary	248 (99.2)	0 (0.0)	2 (0.8)	0 (0.0)	206 (82.4)	1 (0.4)	24 (9.6)	19 (7.6)	201 (80.4)	19 (7.6)	15 (6.0)	15 (6.0)
Splenial	250 (100)	0 (0.0)	0 (0.0)	0 (0.0)	204 (81.6)	1 (0.4)	45 (18.0)	0 (0.0)	138 (55.2)	67 (26.8)	8 (3.2)	37 (14.8)
Surangular	250 (100)	0 (0.0)	0 (0.0)	0 (0.0)	186 (74.4)	10 (4.0)	26 (10.4)	28 (11.2)	113 (45.2)	70 (28.0)	40 (16.0)	27 (10.8)
Working side												
Angular	250 (100)	0 (0.0)	0 (0.0)	0 (0.0)	187 (74.8)	9 (3.6)	30 (12.0)	24 (9.6)	137 (54.8)	59 (23.6)	19 (7.6)	35 (14.0)
Articular	246 (98.4)	1 (0.4)	0 (0.0)	2 (0.8)	144 (57.6)	20 (8.0)	23 (9.2)	62 (24.8)	191 (76.4)	9 (3.6)	33 (13.2)	16 (6.4)
Coronoid	215 (86.0)	9 (3.6)	7 (2.8)	19 (7.6)	110 (44.0)	41 (16.4)	82 (32.8)	17 (6.8)	92 (36.8)	80 (32.0)	51 (20.4)	27 (10.8)
Dentary	249 (99.6)	0 (0.0)	1 (0.4)	0 (0.0)	225 (90.0)	4 (1.6)	5 (2.0)	16 (6.4)	203 (81.2)	15 (6.0)	20 (8.0)	12 (4.8)
Splenial	244 (97.6)	1 (0.4)	2 (0.8)	3 (1.2)	203 (81.2)	4 (1.6)	15 (6.0)	28 (11.2)	159 (63.6)	43 (17.2)	20 (8.0)	28 (11.2)
Surangular	242 (96.8)	1 (0.4)	6 (2.4)	1 (0.4)	158 (63.2)	12 (4.8)	31 (12.4)	49 (19.6)	74 (29.6)	111 (44.4)	35 (14.0)	30 (12.0)

The number of bricks that change the magnitude of principal strain between the stiffest and least stiff trials in each of the three sets. Each bone was sampled by 250 bricks. (+) ε_1 & ε_3 reflects the number of bricks that have increased in both maximum and minimum principal strain, (−) ε_1 & ε_3 reflects the number of bricks that have decreased in both maximum and minimum principal strain, (+) ε_1 (−) ε_3 reflects the number of bricks that have increased in maximum principal strain but decreased in minimum principal strain, (−) ε_1 (+) ε_3 reflects the number of bricks that have decreased in maximum principal strain but increased in minimum principal strain.

Table 3 Number of bricks changing between either dominantly compressive or tensile between the stiffest and least stiff trials in each set.

	Set 1				Set 2				Set 3			
	a (%)	b	c	d (%)	a (%)	b	c	d (%)	a (%)	b	c	d (%)
Balancing side												
Angular	47.6	9	0	−3.6	47.2	15	7	−3.2	47.2	13	12	−0.4
Articular	29.6	2	1	−0.4	34.8	20	7	−5.2	30.8	3	17	**5.6**
Coronoid	70.8	3	2	−0.4	52.8	2	44	**16.8**	71.2	2	12	**4.0**
Dentary	35.6	8	11	**1.2**	41.6	28	15	−5.2	36.0	2	12	**4.0**
Splenial	77.2	10	8	−0.8	54.0	4	60	**22.4**	75.2	14	4	−4.0
Surangular	56.8	1	6	**2.0**	59.2	9	9	0.0	56.0	14	12	−0.8
Total		33	28	−0.3		78	142	4.3		48	69	1.4
Working side												
Angular	55.2	16	1	−6.0	52.0	20	12	−3.2	55.6	18	12	−2.4
Articular	26.8	5	0	−2.0	34.0	29	7	−8.8	27.2	3	26	**9.2**
Coronoid	54.0	26	17	−3.6	28.0	3	55	**20.8**	54.4	13	18	**2.0**
Dentary	49.2	3	7	**1.6**	53.6	18	10	−3.2	49.2	5	11	**2.4**
Splenial	37.2	14	0	−5.6	26.8	9	21	**4.8**	36.0	12	6	−2.4
Surangular	51.2	1	15	**5.6**	56.4	10	12	**0.8**	51.2	21	10	−4.4
Total		65	40	−1.7		89	117	1.9		72	83	0.7

Table showing: (a) the percentage of bricks with ratios of $\varepsilon_1/|\varepsilon_3| > 1$; (b) the number of bricks with ratios of $\varepsilon_1/|\varepsilon_3|$ that change from a value > 1 (indicating tension) to a value < 1 (indicating compression) between the stiffest and least stiff trials in each set; (c) the number of bricks with ratios of $\varepsilon_1/|\varepsilon_3|$ that change from a value < 1 (indicating compression) to a value > 1 (indicating tension) between the stiffest and least stiff trials in each set; (d) the net percentage of bricks changing loading regimes, with negative values indicating compressive forces increasing as stiffness decreases and positive values in bold indicating tensile forces increasing as stiffness decreases.

of total bricks changing between either dominantly compressive or tensile occurred as stiffness decreased in orthotropic bone in set 2, followed by sutures in set 3, and then the isotropic bone in set 1 (Table 3). When comparing bones within each set, each bone responded in different ways to changing material properties. For example, of the bones decreasing in *U* as suture stiffness decreases, the balancing side coronoid became 4% more tensile, the balancing side surangular became 0.8% more compressive, and the working side surangular became 4.4% more compressive.

Changes in the orientation of the principal strain (θ) were also found to occur between sets, with the largest changes in θ associated with set 3 (changes in suture stiffness), followed by set 2 (changes in degree of orthotropy), then set 1 (changes in isotropic stiffness). This trend is also found within most bones considered separately. The exceptions are the working and balancing side dentaries, and the working side splenial, where the greatest change in θ was found in set 2, and the working side coronoid, where the greatest change in θ was found in set 1. When bones are compared within a set, each bone responds differently to changes in stiffness, with $\Delta\theta$ ranging between 3 and 27 radians as isotropic material properties change, between 12 and 28 radians as orthotropic material properties change, and between 12 and 28 radians as suture stiffness changes. In sum, decreases in model stiffness are not always associated with uniform increases in principal strain magnitudes. Changes in degree of bone orthotropy, modeled in set 2, were associated with changes in orientation and relative magnitudes of principal strains indicative of changes in strain regime. This was even more pronounced in set 3, where the effects of changes in suture material properties were examined.

The impact of material properties on the direction of nodal displacement

The magnitude of the difference in nodal displacement between the stiffest and least stiff trials in each set is described by the length of the vectors describing the principal axes of variation in nodal displacement of each bone (i.e. the total least squares regression from principal component one). In all sets, vector length for all balancing side bones is larger than that for the corresponding working side bones in all sets, except the surangulars in set 3 (Table 4).

To assess the direction of the vectors describing the total least squares regression from principal component one, each vector was decomposed into a unit vector. The three axial components describing the unit vector were pooled by axis, and the mean and standard deviation within each bone were calculated. In all sets, decreases in model stiffness resulted in: increased medial deflection of all balancing

Table 4 The magnitude and direction of nodal displacement between the stiffest and least stiff trials in each set.

	Balancing side				Working side			
	x (*s*)	*y* (*s*)	*z* (*s*)	Length (*s*)	*x* (*s*)	*y* (*s*)	*z* (*s*)	Length (*s*)
Angular								
Set 1	−0.621 (0.132)	0.399 (0.542)	0.321 (0.203)	43.24 (28.10)	0.442 (0.278)	0.425 (0.568)	0.457 (0.129)	22.53 (12.03)
Set 2	−0.503 (0.158)	0.445 (0.528)	0.366 (0.336)	22.79 (16.89)	0.161 (0.283)	0.491 (0.559)	0.529 (0.247)	10.17 (6.54)
Set 3	−0.500 (0.143)	0.444 (0.589)	0.385 (0.194)	16.06 (9.55)	0.417 (0.197)	0.460 (0.597)	0.441 (0.160)	9.99 (5.46)
Articular								
Set 1	−0.469 (0.339)	−0.336 (0.543)	0.378 (0.341)	3.60 (3.06)	0.481 (0.308)	−0.351 (0.514)	0.415 (0.339)	3.12 (2.51)
Set 2	−0.302 (0.249)	−0.333 (0.454)	0.601 (0.409)	1.72 (1.30)	0.276 (0.218)	−0.349 (0.450)	0.627 (0.400)	1.54 (1.06)
Set 3	−0.242 (0.434)	−0.475 (0.523)	0.209 (0.459)	1.56 (1.44)	0.217 (0.424)	−0.472 (0.525)	0.121 (0.502)	1.14 (1.06)
Coronoid								
Set 1	−0.304 (0.126)	0.941 (0.037)	0.060 (0.024)	56.15 (5.69)	0.180 (0.114)	0.924 (0.034)	0.311 (0.048)	28.90 (1.93)
Set 2	−0.276 (0.109)	0.954 (0.027)	−0.018 (0.017)	31.81 (3.49)	0.051 (0.091)	0.947 (0.015)	0.300 (0.048)	13.71 (0.84)
Set 3	−0.258 (0.122)	0.945 (0.040)	0.144 (0.057)	19.93 (1.72)	0.193 (0.097)	0.940 (0.037)	0.251 (0.07)	12.34 (0.79)
Dentary								
Set 1	−0.388 (0.083)	0.914 (0.038)	0.052 (0.051)	98.69 (22.02)	−0.309 (0.121)	0.928 (0.023)	0.145 (0.079)	76.87 (33.25)
Set 2	−0.497 (0.094)	0.860 (0.044)	0.016 (0.051)	53.79 (9.68)	−0.475 (0.121)	0.858 (0.056)	0.123 (0.075)	43.01 (18.87)
Set 3	−0.200 (0.058)	0.972 (0.021)	0.087 (0.055)	38.99 (9.80)	−0.129 (0.091)	0.978 (0.011)	0.117 (0.074)	31.72 (12.44)
Splenial								
Set 1	−0.401 (0.087)	0.909 (0.039)	0.045 (0.029)	90.99 (13.43)	−0.227 (0.169)	0.920 (0.016)	0.258 (0.084)	54.67 (20.07)
Set 2	−0.492 (0.084)	0.865 (0.043)	−0.008 (0.024)	50.39 (6.24)	−0.445 (0.149)	0.834 (0.049)	0.272 (0.089)	28.49 (12.29)
Set 3	−0.227 (0.084)	0.962 (0.029)	0.112 (0.044)	34.18 (6.10)	−0.060 (0.136)	0.966 (0.022)	0.195 (0.078)	23.74 (7.42)
Surangular								
Set 1	−0.255 (0.285)	0.499 (0.692)	0.171 (0.313)	8.08 (17.43)	0.157 (0.290)	0.538 (0.686)	0.175 (0.319)	13.65 (11.22)
Set 2	−0.167 (0.207)	0.575 (0.620)	0.198 (0.419)	4.74 (10.39)	0.039 (0.219)	0.610 (0.629)	0.184 (0.387)	7.35 (6.04)
Set 3	−0.178 (0.232)	0.608 (0.665)	0.079 (0.313)	3.30 (6.50)	0.118 (0.206)	0.657 (0.627)	−0.002 (0.347)	6.49 (4.62)

Table summarizing the data from the primary axis of variation of nodal displacement. '*x*', '*y*' and '*z*' columns represent the three components of a unit vector describing the primary axis of variation of nodal displacement. The values reported in these columns reflect the mean value from the 500 sub-sampled nodes (standard deviations are in parentheses). These values indicate the primary direction of displacement. The 'Length' column represents the length of a vector calculated from a total least squares regression on the displacement data. The values reported in this column reflect the means values from the 500 sub-sampled nodes (standard deviations are in parentheses). This column indicates the magnitude of nodal displacement as stiffness is decreased. All values are reported in mm $\times 10^{-3}$.

side bones; increased medial deflection of the working side angular, articular, coronoid and surangular; increased lateral deflection of the working side dentary and splenial; increased dorsal deflection of all bones except the working and balancing articulars; increased ventral deflection of the articulars; and increased rostral displacement of all bones, except the balancing side coronoid in set 2, the balancing side splenial in set 2, and the working side surangular in set 3 (Table 4). These latter three bones display changes in polarity of the displacement vector between sets, indicating that variation in material properties can result in changes in the nature of the deformation regime. Changes in the relative magnitudes of the unit vectors between sets also suggest complex effects of material properties on model behavior. To highlight two examples, in set 2 the working and balancing side dentary and splenial show decreased vertical and increased transverse displacement compared with set 1 and set 3. These data indicate that the direction and magnitude of model displacement resulting from changes in the stiffness matrix are distinct in each of the three sets.

Discussion

The aim of this study was to evaluate the impact of bone and suture material properties on strain, stress and deformation regimes in the vertebrate skeleton. The effect of changes in stiffness in isotropic bone, orthotropic bone and suture stiffness were examined.

The effects of decreasing stiffness in isotropic bone

In the first set, the mandible was modeled as linear elastic isotropic bone with no sutures, and the stiffness of the bone material was varied. We predicted that decreasing the stiffness of isotropic bone with no sutures would result in increases in the magnitude of principal strains, and little change in either the orientation of maximum principal

Table 5 The average change in the orientation of maximum principal strain between the stiffest and least stiff trials in each set.

	Set 1 (*s*)	Set 2 (*s*)	Set 3 (*s*)
Balancing side			
Angular	0.11 (0.19)	0.21 (0.24)	0.22 (0.31)
Articular	0.07 (0.13)	0.19 (0.22)	0.28 (0.35)
Coronoid	0.03 (0.04)	0.11 (0.11)	0.17 (0.22)
Dentary	0.09 (0.11)	0.19 (0.18)	0.12 (0.18)
Splenial	0.07 (0.12)	0.12 (0.14)	0.12 (0.19)
Surangular	0.07 (0.09)	0.18 (0.23)	0.20 (± 0.23)
Working side			
Angular	0.10 (0.12)	0.18 (0.24)	0.20 (0.26)
Articular	0.14 (0.22)	0.21 (0.28)	0.25 (0.32)
Coronoid	0.27 (0.29)	0.21 (0.21)	0.22 (0.24)
Dentary	0.13 (0.18)	0.20 (0.26)	0.13 (0.22)
Splenial	0.17 (0.22)	0.28 (0.33)	0.21 (0.25)
Surangular	0.11 (0.17)	0.20 (0.23)	0.23 (0.25)
Total	0.10 (0.16)	0.19 (0.24)	0.21 (0.28)

Table showing the mean difference in radians of the orientation of maximum principal strain between the least stiff and stiffest trials. Standard deviations are in parentheses.

strain or the direction of nodal displacement. As expected, decreases in the stiffness of linear elastic isotropic bone in a model without sutures resulted in increases in stored elastic energy, and in the magnitudes of maximum and minimum principal strain in nearly all bricks in all bones (Table 2). However, contrary to the predictions of H_1, decreasing stiffness did result in some bricks changing from being predominantly compressive or tensile [3.6% of balancing side bricks and 6.0% of working side bricks (Table 3)]. In addition, the orientation of maximum principal strain was found to change as stiffness was decreased, with an average of a 0.10 radian (s = 0.16) difference between the stiffest and least stiff conditions in this set (Table 5).

Thus, decreases in isotropic stiffness in the model not only result in changes in the magnitude of the principal strain but also the nature of the mandible's strain regime in a small number of nodes. Such changes are unexpected when linear elastic isotropic material properties are varied within a body, and may reflect variation in the superimposition of applied forces as areas of concentrated stress expand in response to lower material stiffness. In support of this claim, of the bricks not increasing in the magnitude of principal strain, most were increasing in one component of principal strain while decreasing in the other [i.e. these bricks were becoming either increasingly more tensile or compressive (Table 2)].

Alternatively, these changes could reflect modeling artifact. Although suture material properties were not modeled in set 1, the mesh geometry in bricks representing suture locations are identical in all sets, differing only in the material properties. The complex geometry of these suture areas may have generated undesirable brick aspect ratios or other meshing artifacts. Meshing artifacts such as these, referred to as discretization errors, typically manifest themselves as concentrated areas of stress and strain, and may have impacted the behavior of the model in unpredictable ways.

The effects of decreasing stiffness in orthotropic bone

In the second set, the mandible was modeled as linear elastic orthotropic bone with no sutures, and the stiffness of the bone material was varied along the rostrocaudal axis of the mandible. We predicted that decreasing the stiffness of orthotropic bone in a model with no sutures would result in an increase in the *magnitude* of stored elastic energy and principal strains, with a greater impact on the orientation of maximum principal strain and the direction of nodal displacement than seen in set 1. As predicted by H_2, decreases in the stiffness of orthotropic bone with no sutures did result in an increase in stored elastic energy in all bones (Table 1). Also as predicted by H_2, the majority of bricks experienced an increase in the magnitude of principal strain as stiffness decreased (Table 2). However, the percentage of bricks increasing in the magnitude of principal strain was lower in set 2 than in set 1. This is the result of a greater number of bricks either decreasing in their magnitude of principal strain, or increasing in one component of principal strain while decreasing in the other as stiffness decreased. Of those bricks not increasing in their magnitude of principal strain, a larger percentage increased in one component of principal strain while decreasing in the other [i.e. became associated with either more compressive or more tensile principal strains as stiffness decreased (Table 2)].

Further supporting the claim that changes in orthotropic material properties result in changes in the nature of the strain regime, a number of elements changed between being either predominantly compressive or tensile (Table 3). The orientation of principal strains also changed, with an average difference of 0.19 radians (s = 0.24) between the stiffest and least stiff conditions (Table 5). In both of these measures of strain, changes are larger than for those in set 1.

Changes in the deformation regime in set 2 were also found to diverge from those of set 1, with the primary direction of nodal displacement switching from rostral in set 1 to caudal in set 2 in both the balancing side coronoid and splenial. Moreover, the relative contributions of each component of the unit vector differ between set 1 and set 2 for all bones, indicating shifts in the direction of nodal displacement in response to decreasing stiffness (Table 4).

As in the isotropic condition of set 1, it remains unknown if the changes indicative of variation in strain and deformation regimes discussed here are biologically relevant or are instead modeling artifact. However, given that a greater number of bricks in the orthotropic condition of set 2,

when compared with the isotropic condition of set 1: become increasingly compressive or tensile, change between being either dominantly compressive or tensile, and have a larger difference in the orientation of maximum principal strain, we conclude that changing the stiffness in an orthotropic material will result in changes to both the strain and deformation regimes within that body. Because many vertebrate bones are orthotropic, including the mandible of *Alligator* (Zapata et al. 2010), this conclusion highlights the importance of using precise material properties when constructing and drawing conclusions from a FEM.

The effects of decreasing stiffness in sutures

In the third set, the mandible was modeled as linear elastic isotropic bone with sutures between the bones. The stiffness of the sutures was varied, while the stiffness of the bones was held constant. We predicted that decreasing suture stiffness would result in either no change or a decrease in the magnitude of stored elastic energy and principal strains within the bones as more and more of the strain energy was absorbed by the sutures. Contrary to our expectations, decreases in suture stiffness resulted in *increases* in stored elastic energy (*U*) in most of the bones in the mandible, with the exception of the working and balancing side surangulars and the balancing side coronoid (Table 1). Of the bones increasing in *U*, the majority of bricks increased their principal strain magnitudes; however, the number of bricks either decreasing in principal strain magnitudes or increasing in the magnitude of one component of principal strain while decreasing in the other was greater than in set 1. Of the bones decreasing in *U*, the majority of the bricks in the balancing side coronoid and working side surangular *decreased* in principal strain magnitude. In the balancing side surangular, the majority of the bricks *increased* in principal strain magnitude (Table 2). In all bones in set 3, the number of bricks increasing in one component of principal strain and a decrease in the other, i.e. non-suture bricks becoming more compressive or tensile as suture stiffness decreased, was greater than set 1 but roughly equivalent with set 2.

Also indicative of strain regime changing with decreasing suture stiffness, a number of non-suture bricks changed between either dominantly compressive or tensile as suture stiffness decreased (Table 3). In addition, the orientation of principal strains changed with an average difference of 0.21 radians (s = 0.28) between the stiffest and least stiff conditions in this set, very similar to the average value for set 2 (Table 5).

Changes in the strain regime also manifest themselves in the deformation regime as changes in the direction of displacement of individual bones. Decreasing suture stiffness results in small caudal displacement of the working side surangular, whereas decreasing in the material property defining sets 1 and 2 results in rostral displacements. The relative contributions of each component of the unit vector differ between set 1 and set 3 for all bones as well, indicating shifts in the direction of nodal displacement in response to decreasing stiffness. To cite one example, the working side articular displaces primarily in the medial direction in set 1 and ventrally in set 3 (Table 4).

Just as in the discussion of sets 1 and 2, it is impossible to rule out that these values reflect meshing error; however, given that a greater number of bricks in set 3 than in set 1 became increasingly compressive or tensile, changed between being either dominantly compressive or tensile, and had larger differences in the orientation of maximum principal strain, we conclude that changing the stiffness of sutures can result in changes to strain and deformation regimes within that body. Because most vertebrate skulls and non-mammalian mandibles have patent sutures, this conclusion highlights the importance of including sutures in FEMs with precise material properties.

The impact of sutures on global measures of model behavior might be mitigated if the largest changes are found in localized areas. Localized stress concentrations are expected at the interface of two materials with a sharp gradient in material properties. This phenomenon is the result of a condition known as a *bimaterial interface* (Shilkrot & Srolovitz, 1998; Thomopoulos et al. 2003). To determine if the differences in measures of principal strain reported here occur exclusively in areas of concentrated stress or are instead distributed more evenly throughout the bones, a *post-hoc* analysis relating measures of principal strain to the distance of each brick to the sutures was performed.

Does the distance of each brick to the nearest suture impact the magnitude and orientation of maximum principal strain?

As previously discussed, decreases in a bone's value of *U* as suture stiffness decreases is a plausible indicator for elastic energy being stored in adjacent sutures. Data from the working and balancing side surangulars are considered in this *post-hoc* analysis because, in addition to decreases in suture stiffness being associated with decreases in *U* for both bones, the majority of bricks in the working side surangular decreased in principal strain magnitude whereas the majority of bricks in the balancing side surangular increased in principal strain magnitude.

To determine if these changes in principal strain magnitude occur near the bone–suture interface, or are instead more broadly dispersed throughout the bone, the distance of every brick to the nearest suture (D_{ns}) was calculated and then plotted against: the magnitude of maximum principal strain in the stiffest trial of each set (ε_{1t1}); the difference in the magnitude of maximum principal strain between the least stiff and stiffest trials ($\Delta\varepsilon_1$); and the difference in the orientation of maximum principal strain between the least stiff and stiffest trials ($\Delta\theta$).

In set 1, the largest values of ε_{1t1} and $\Delta\varepsilon_1$ in the working and balancing side surangulars are found at small values of D_{ns} [i.e. adjacent to the bone/suture interface (Fig. 5)]. Moreover, nearly all values of $\Delta\varepsilon_1$ are positive, indicating that maximum principal strain increases in these areas as stiffness is decreased (Table 2). In set 2, the largest values of ε_{1t1} and $\Delta\varepsilon_1$ for the balancing side surangular are grouped near the smallest values of D_{ns}, but the largest values of $\Delta\varepsilon_1$ in the working side surangular are not (Table 2). In set 3, the largest values of ε_{1t1} and $\Delta\varepsilon_1$ are found at small values of D_{ns} just as in set 1; however, they are negative (Table 2). In sum, these data indicate that although the model analyzed in set 1 did not include sutures (i.e. the bricks representing suture locations were given the material properties of the surrounding bone), the highest values of ε_{1t1} and $\Delta\varepsilon_1$ are found near the bricks representing suture locations. Decreasing the stiffness of sutures in set 3 resulted in a decrease in $\Delta\varepsilon_1$ near the sutures, i.e. within the same bricks that experience an increase in $\Delta\varepsilon_1$ in the isotropic condition of set 1.

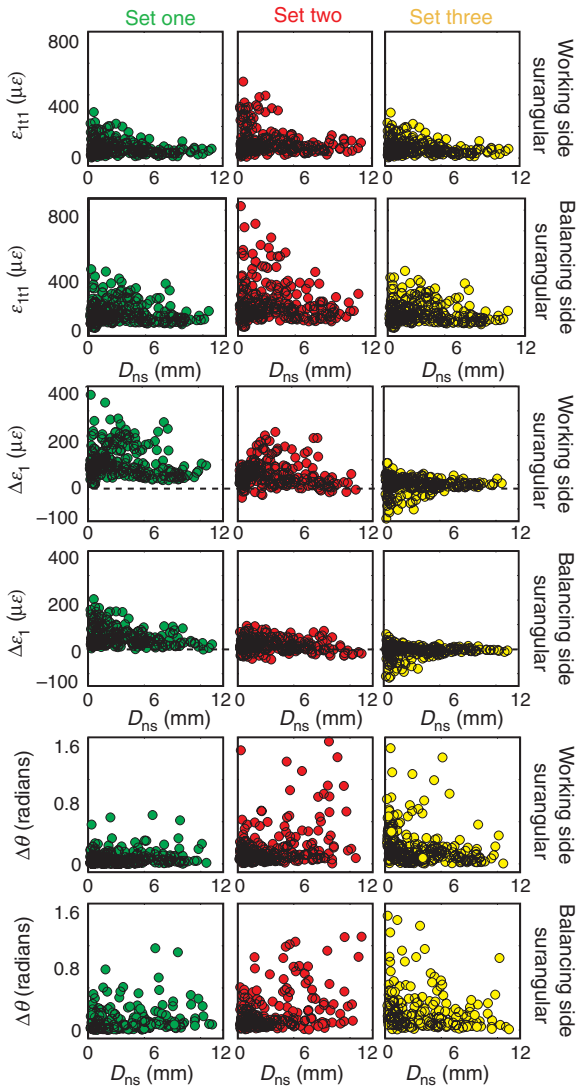

Fig. 5 Scatter plot showing the relationship between the distance of each brick to a suture (D_{ns}) with magnitude of maximum principal strain in the stiffest trial in each set (ε_{1t1}), the difference in the magnitude of maximum principal strain between the stiffest and least stiff conditions in each set ($\Delta\varepsilon_1$), and the difference in the orientation of maximum principal strain between the stiffest and least stiff conditions in each set ($\Delta\theta$). Set 1 is represented by green, set 2 is represented by red, and set 3 is represented by yellow. This plot shows that the largest values of ε_{1t1} are found at small values of D_{ns} in all sets. The largest values of $\Delta\varepsilon_1$ are found at small values of D_{ns} in set 1, on the balancing side in sets 2 and 3, and at high values of D_{ns} in the balancing side of set 2. The largest values of $\Delta\theta$ are found at small values of D_{ns} in sets 1 and 3, and high values of D_{ns} in set 2.

The largest values of $\Delta\theta$ in sets 1 and 3 are found close to sutures (i.e. at very small values of D_{ns}), whereas the largest values of $\Delta\theta$ in set 2 are found at high values of D_{ns}. On average, set 3 had the largest values of $\Delta\theta$ (Table 5). Taken together, we conclude that the impact of suture stiffness on $\Delta\theta$ is highest adjacent to sutures, and that suture stiffness impacts $\Delta\theta$ in these areas more than changes in stiffness of isotropic bone and orthotropic bone.

Large values of $\Delta\varepsilon_1$ and $\Delta\theta$ are not unexpected in areas of concentrated strain. In all sets, the highest values of ε_{1t1} are found at low values of D_{ns}, indicating that strain might be concentrating in this region. As previously discussed, it is not unexpected to have concentrated areas of stress and strain at the bone/suture interface when it is modeled as a bimaterial interface. Somewhat unexpected are the large values of ε_{1t1} and $\Delta\varepsilon_1$ at low values of D_{ns} in set 1, despite the suture locations in this set being given the material properties of the surrounding bone. As previously mentioned, the complex geometry of these sutures may have generated undesirable brick aspect ratios or other meshing artifacts, referred to as discretization errors. Such errors may explain the concentrated areas of stress and strain at these suture locations in set 1. Convergence testing has been shown to mitigate the effects of discretization error on certain model performance criteria (Hart, 1989; Schmidt et al. 2009); however, not universally for all variables (Cook et al. 2001; Schmidt et al. 2009). The trends discussed here for the working and balancing side surangulars are largely representative of all bones in the mandible, making discretization error a possible explanation of these results.

A more intriguing explanation is that sutures in the *Alligator* mandible are located in positions that, in their absence, tend to concentrate stress and strain by virtue of their geometry. Further analyses of these theoretical data, considered in conjunction with convergence testing and independent *in vivo* experimental data, are necessary before any conclusive statements can be made on this point (Richmond et al. 2005).

Biological implications

The presence of localized stress concentrations near sutures is not a surprising result, and indeed similar results

have been reported in the FEA of several taxa when sutures are included (Kupczik et al. 2007; Fitton et al. 2009; Moazen et al. 2009). What remains unclear is if the strain, and the associated stress, distribution at the bone/suture interface is of a biologically realistic magnitude. Modeling bone/suture interfaces with a sharp gradient in the material properties may lead to artifactually high and localized principal stresses. This is due to the fact that many biological bimaterial interfaces, such as bone/tendon or bone/suture interfaces, adopt a strategy of functional grading (Enlow, 1968, 1990; Woo et al. 1987; Thomopoulos et al. 2003; Buehler, 2007; Buehler & Ackbarow, 2008), where the transition between the material properties of the bimaterial is graduated (Thomopoulos et al. 2003; Birman & Byrd, 2007). Functional grading in both biological (Thomopoulos et al. 2006) and non-biological materials (Birman & Byrd, 2007) has been shown to improve residual stress distributions.

In vivo and *in vitro* analysis of cranial strain measurements in a number of different taxa support the results reported here as biologically plausible. Numerous studies have found that principal strain magnitudes over sutures are considerably higher than the surrounding bones (Behrents et al. 1978; Oudhof & Doorenmaalen, 1983; Smith & Hylander, 1985; Herring & Mucci, 1991; Herring, 1993; Rafferty & Herring, 1999; Herring & Teng, 2000; Rafferty et al. 2003; Sun et al. 2004; Popowics & Herring, 2007). This suggests that a localized stress distribution exists at bone margins that might degrade as the total distance to a suture is increased. Additional *in vivo* and *in vitro* work is needed to understand if the localized stress distributions at the bone/suture interface, as modeled here, are of a biologically meaningful magnitude.

Large strain magnitudes over sutures have been used to argue that sutures are acting as strain sinks, storing elastic energy, thereby decreasing stress, and the associated strain, in the surrounding bone (Pritchard et al. 1956; Buckland-Wright, 1972, 1978; Jaslow, 1990; Rafferty et al. 2003). Our modeling data provide evidence in support of this idea. Stored elastic energy was calculated for the entire mandible both including and excluding sutures. In the least stiff trial of set 3, it was found that including sutures resulted in a 17.1% difference in stored elastic energy on the balancing side and a 16.5% difference in stored elastic energy on the working side. In sets 1 and 2, there is only a 7.5% difference in stored elastic energy, likely reflecting changes in U resulting from an increase in the measured volume (Table 1). Therefore, the percentage increase when sutures are added to the calculation of U in set 3 is larger than would be predicted from just an increase in the measured volume.

We expected that by adding sutures in set 3, stored elastic energy in each of the bones of the mandible would go down as the sutures absorbed strain energy. However, this result was only observed in three out of the 12 bones: the working and balancing side surangulars and the balancing side coronoid (Table 1). In these three bones, not only did stored elastic energy decrease, but principal strain magnitudes decreased adjacent to the bone/suture interface. The remaining nine bones of the mandible experienced increases in stored elastic energy when sutures were added (Table 1), with the majority of bricks increasing in their principal strain magnitudes.

This highlights the importance of selecting the appropriate performance measure when assigning optimization criteria to a biological structure, i.e. the material properties driving mechanical behavior near the bone/suture interface of the surangular may be different from those of the dentary. As pointed out by Farke (2008), a sutural zone, defined as a suture and the surrounding bone, may be a more appropriate functional unit when attempting to assign optimality criteria to bony elements. Defining functional units in this manner allows hypotheses related to varied performance demands throughout the structure to be tested explicitly.

Varied performance demands within a functional unit such as the *Alligator* mandible are of particular interest in the context of mechanobiology. Exogenously applied cyclic loads have been shown to be osteogenic at suture boundaries (Kopher & Mao, 2003; Byron et al. 2004; Byron, 2006), suggesting that the loading environment experienced throughout ontogeny may contribute to the phenotypic variation of the mandible and skull. The data presented here highlight the importance of precisely characterizing the gradients of strain distributions on and around sutures, including how both the magnitude and orientation of principal strain changes as a function of the distance to the bone/suture interface. Only after the behavior of stress and strain gradients approaching the bone/suture interface are characterized and placed in the appropriate context of performance can hypotheses relating ontogenetic changes in suture morphology to loading environment be addressed.

Practical implications for FEA

The accurate measurement of material properties across complex biological structures, like the mandible studied here, is difficult and time-consuming in living animals, and impossible in fossils. This makes it important to determine the potential impact that bone material properties can have on stress and strain in vertebrate bones, not only to improve understanding of bone deformation in living vertebrates, but also to aid modeling and interpretation of fossils.

The data presented here demonstrate that variation in the orthotropic material properties of bone and isotropic material properties of sutures impact more than just the magnitude of principal strains. Compared with variation in the isotropic material properties of bone, variation in the orthotropic material properties of bone and isotropic material properties of sutures resulted in: a greater number of bricks becoming either more compressive or more tensile; bricks

changing between being either dominantly compressive or tensile; and larger changes in the orientation of maximum principal strain. In addition, multivariate analysis of model displacement revealed changes in both the magnitude and direction resulting from changes in material properties. Taken together, we conclude that variation in both the orthotropic material properties of bone and the isotropic material properties of sutures results in changes not only to the overall magnitude of principal strain but also to the nature of the strain and deformation regimes in the body.

Model validation using either *in vivo* or *in vitro* methods is the only way of placing this variation in the context of model accuracy and, indeed, acceptable levels of error may vary depending on the question being asked. The largest variations in ε_{1t1}, $\Delta\varepsilon_1$ and $\Delta\theta$ reported here tended to occur adjacent to the bone/suture interface in both the isotropic condition of set 1 and the suture stiffness condition of set 3. However, this was not universally true. Variation in orthotropic material properties resulted in the largest values of $\Delta\varepsilon_1$ (on the working side surangular) and $\Delta\theta$ (on both the working and balancing sides) at large values of D_{ns}. For this reason, we caution the reader from interpreting these results as a method of avoiding error prone areas such as the bone/suture interface when sampling results from a FEM with approximate material properties.

For models that cannot be validated, such as those from extinct organisms, the accuracy of statements concerning the behavior of the model must be considered in the context of the accuracy of the material properties used. Material properties from the bones of extinct organisms can be estimated using both phylogenetic bracketing and histological methods (Rayfield et al. 2001; Erickson et al. 2002). Implicit in both these methods is a need for large comparative datasets, highlighting the importance of comparative materials testing in vertebrate bone.

Conclusion

Variation in the isotropic material properties of bone with no sutures resulted primarily in changes within the magnitude of principal strain, whereas variation in the orthotropic material properties of bone and the isotropic material properties of sutures resulted in changes to the strain and deformation regimes of the model. This conclusion highlights the importance of using biologically verified material properties when modeling the vertebrate skeleton.

Comparisons of bones within each set revealed that each bone responds in a different way to changing material properties. When suture stiffness was decreased, the balancing side coronoid and working and balancing side surangulars decreased in stored elastic energy, whereas the remaining nine bones of the mandible increased in stored elastic energy. These data highlight the importance of defining the appropriate functional unit when addressing relationships of performance and morphology.

The decrease in stored elastic energy in the balancing side coronoid and working side surangular was accompanied by a decrease in the magnitude of principal strain. These large differences in the magnitude of principal strain were found to occur adjacent to the bone/suture interface. Taken together, these data suggest that sutures are storing strain energy, thereby decreasing the stored elastic energy and magnitude of principal strain within some bones. These modeling data fail to falsify the hypothesis that a functional consequence of patent sutures is the ability to store elastic energy, and thereby decrease the magnitude of principal strain within bones.

References

Anapol F, Barry K (1996) Fiber architecture of the extensors of the hindlimb in semiterrestrial and arboreal guenons. *Am J Phys Anthropol* **99**, 429–447.

Behrents RG, Carlson DS, Abdelnour T (1978) *In vivo* analysis of bone strain about the sagittal suture in *Macaca mulatta* during masticatory movements. *J Dent Res* **57**, 904–908.

Biewener AA, Taylor CR (1986) Bone strain: a determination of gait and speed. *J Exp Biol* **123**, 383–400.

Birman V, Byrd LW (2007) Modeling and analysis of functionally graded materials and structures. *Appl Mech Rev* **60**, 195–215.

Buckland-Wright JC (1972) The shock absorbing effect of cranial sutures in certain mammals. *J Dent Res* **51**, 1241.

Buckland-Wright JC (1978) Bone structure and the patterns of force transmission in the cat skull (*Felis catus*). *J Morphol* **155**, 35–62.

Buehler MJ (2007) Molecular nanomechanics of nascent bone: fibrilar toughening by mineralization. *Nanotechnology* **18**, 1–9.

Buehler MJ, Ackbarow T (2008) Nanomechanical strength mechanisms of hierarchical biological materials and tissues. *Comput Methods Biomech Biomed Engng* **11**, 595–607.

Byron CD (2006) The role of osteoclast in cranial suture waveform patterning. *Anat Rec A Discov Mol Cell Evol Biol* **288**, 552–563.

Byron CD, Borke J, Yu J et al. (2004) Effects of increased muscle mass on mouse sagittal suture morphology and mechanics. *Anat Rec A Discov Mol Cell Evol Biol* **279**, 676–684.

Carter DR, Beaupre GS (2001) *Skeletal Function and Form: Mechanobiology of Skeletal Development, Aging and Regeneration*. New York: Cambridge University Press.

Cook R, Malkus D, Lesha M et al. (2001) *Concepts and Applications of Finite-Element Analysis*. New York: John Wiley.

Currey JD (1979) Mechanical properties of bone with greatly differing functions. *J Biomech* **12**, 313–319.

Currey JD (1987) The evolution of mechanical properties of amniote bone. *J Biomech* **20**, 1035–1044.

Currey JD (1999) The design of mineralized hard tissues for their mechanical functions. *J Exp Biol* **202**, 3285–3294.

Currey JD (2002) *Bones: Structure and Mechanics*. Princeton: Princeton University Press.

Dumont ER, Grosse I, Slater GJ (2009) Requirements for comparing the performance of finite element models of biological structures. *J Theor Biol* **256**, 96–103.

Enlow DH (1968) *The Human Face: An Account of the Postnatal Growth and Development of the Craniofacial Sutures*. New York: Harper and Row.

Enlow DH(1990) *Handbook on Facial Growth*. Philadelphia: W.B. Saunders.

Erickson G, Catanese J, Keaveny T (2002) Evolution of the biomechanical material properties of the femur. *Anat Rec* **268**, 115–124.

Farke AA (2008) Frontal sinuses and head-butting in goats: a finite element analysis. *J Exp Biol* **211**, 3085–3094.

Fitton LC, Kupczik K, Milne N, et al. (2009) The role of sutures in modulating strain distribution within the skull of *Macaca fascicularis*. *Am J Phys Anthropol* **138**(S48), 189.

Grosse I, Dumont ER, Coletta C et al. (2007) Techniques for modeling muscle-induced forces in finite element models of skeletal structures. *Anat Rec* **290**, 1069–1088.

Hart R (1989) In *The finite-element method. In: Bone Mechanics* (ed Cowin S), pp. 53–74. Boca Raton: CRC Press.

Herring SW (1993) Formation of the vertebrate face epigenetic and functional influences. *Am Zool* **33**, 472–483.

Herring SW, Mucci RJ (1991) *In vivo* strain in cranial sutures: the zygomatic arch. *J Morphol* **207**, 225–239.

Herring SW, Teng S (2000) Strain in the braincase and its sutures during function. *Am J Phys Anthropol* **112**, 575–593.

Hibbeler RC(2004) *Mechanics of Materials*. Upper Saddle River, New Jersey: Prentice Hall. 528 pp.

Holliday CM (2009) New insights into the dinosaur jaw muscle anatomy. *Anat Rec* **292**, 1246–1265.

Holliday CM, Witmer LM (2007) Archosaur adductor chamber homology: integration of musculoskeletal and topological criteria in jaw muscle homology. *J Morphol* **268**, 457–484.

Hubbard RP (1971) Flexure of layered cranial bone. *J Biomech* **4**, 251–263.

Hylander WL (1984) Stress and strain in the mandibular symphysis of primates: a test of competing hypotheses. *Am J Phys Anthropol* **64**, 1–46.

Hylander WL, Johnson KR (1994) Jaw muscle function and wishboning of the mandible during mastication in macaques and baboons. *Am J Phys Anthropol* **94**, 523–547.

Hylander WL, Picq PG, Johnson KR (1991) Masticatory-stress hypotheses and the supraorbital region of primates. *Am J Phys Anthropol* **86**, 1–36.

Jaslow CR (1990) Mechanical properties of cranial sutures. *J Biomech* **23**, 313–321.

Jaslow CR, Biewener AA (1995) Strain patterns in the horncores, cranial bones and sutures of goats (*Capra hircus*) during impact loading. *J Zool (Lond)* **235**, 193–210.

Kopher R, Mao J (2003) Suture growth modulated by the oscillatory component of micromechanical strain. *J Bone Miner Res* **18**, 521–528.

Kupczik K, Dobson C, Fagan MJ et al. (2007) Assessing mechanical function of the zygomatic region in *macaques*: validation and sensitivity testing of finite element models. *J Anat* **210**, 41–53.

Marinescu R, Daegling DJ, Rapoff AJR (2005) Finite-element modeling of the anthropoid mandible: the effects of altered boundary conditions. *Anat Rec A Discov Mol Cell Evol Biol* **238A**, 300–309.

Metzger KA, Daniel WTJ, Ross CF (2005) Comparison of beam theory and finite-element analysis with *in vivo* bone strain from the alligator cranium. *Anat Rec* **283A**, 331–348.

Moazen M, Curtis N, O'Higgins P et al. (2009) Assessment of the role of sutures in a lizard skull: a computer modelling study. *Proc Biol Sci* **276**, 39–46.

Moss ML, Meehan M, Salentjin L (1972) Transformative and translative growth processes in neurocranial development of the rat. *Acta Anat* **81**, 161–182.

Murphy RA, Beardsley AC (1974) Mechanical properties of the cat soleus muscle *in situ*. *Am J Physiol* **227**, 1008–1013.

Nowlan N, Murphy P, Prendergast PJ (2007) Mechanobiology of embryonic limb development. *Ann N Y Acad Sci* **1101**, 389–411.

Nowlan N, Murphy P, Prendergast PJ (2008) A dynamic pattern of mechanical stimulation promotes ossification in avian embryonic long bones. *J Biomech* **41**, 249–258.

Oudhof HA, Doorenmaalen WJ (1983) Skull morphogenesis and growth: hemodynamic influence. *Acta Anat (Basel)* **117**, 181–186.

Papadimitriou HM, Swatz SM, Kunz TM (1996) Ontogenetic and anatomic variation in mineralization of the wing skeleton of the Mexican free-tailed bat, *Tadarida brasiliensis*. *J Zool (Lond)* **240**, 411–426.

Persson M (1995) The role of sutures in normal and abnormal craniofacial growth. *Acta Odontol Scand* **53**, 152–161.

Peterson J, Dechow PC (2002) Material properties of the inner and outer cortical tables of the human parietal bone. *Anat Rec* **268**, 7–15.

Popowics TE, Herring SW (2007) Load transmission in the nasofrontal suture of the pig, *Sus scrofa*. *J Biomech* **40**, 837–844.

Pritchard JJ, Scott JH, Girgis FG (1956) The structure and development of cranial and facial sutures. *J Anat* **90**, 73–86.

Radhakrishnan P, Mao JJ (2004) Nanomechanical properties of facial sutures and sutural mineralization front. *J Dent Res* **83**, 470–475.

Rafferty KL, Herring SW (1999) Craniofacial sutures: morphology, growth, and *in vivo* masticatory strains. *J Morphol* **242**, 167–179.

Rafferty KL, Herring SW, Marshall CD (2003) Biomechanics of the rostrum and the role of facial sutures. *J Morphol* **257**, 33–44.

Ravosa MJ, Noble VE, Hylander WL et al. (2000) Masticatory stress, orbital orientation and the evolution of the primate postorbital bar. *J Hum Evol* **38**, 667–693.

Rayfield EJ (2005) Using finite-element analysis to investigate suture morphology: a case study using large carnivorous dinosaurs. *Anat Rec A Discov Mol Cell Evol Biol* **283A**, 349–365.

Rayfield EJ, Norman DB, Horner CC et al. (2001) Cranial design and function in a large theropod dinosaur. *Nature* **409**, 1033–1037.

Richmond BG, Wright BW, Grosse I et al. (2005) Finite element analysis in functional morphology. *Anat Rec A Discov Mol Cell Evol Biol* **283A**, 259–274.

Ross CF (2001) *In vivo* function of the craniofacial haft: the interorbital ''pillar''. *Am J Phys Anthropol* **116**, 108–139.

Ross CF (2005) Finite element analysis in vertebrate biomechanics. *Anat Rec A Discov Mol Cell Evol Biol* **283A**, 253–258.

Ross CF, Metzger KA (2004) Bone strain gradients and optimization in vertebrate skulls. *Ann Anat* **186**, 387–396.

Ross CF, Patel BA, Slice DE et al. (2005) Modeling masticatory muscle force in finite element analysis: sensitivity analysis

using principal coordinates analysis. *Anat Rec A Discov Mol Cell Evol Biol* **283A**, 288–299.

Rubin C, Lanyon L (1984) Regulation of bone formation by applied dynamic loads. *J Bone Joint Surg Am* **66**, 397–402.

Schmidt H, Alber T, Wehner T et al. (2009) Discretization error when using finite element models: analysis and evaluation of an underestimated problem. *J Biomech* **42**, 1926–1934.

Schwartz-Dabney CL, Dechow PC (2002) Accuracy of elastic property measurement in mandibular cortical bone is improved by using cylindrical specimens. *J Biomech Engng* **124**, 714–723.

Sellers WL, Crompton RH (2004) Using sensitivity analysis to validate the predictions of a biomechanical model of bite forces. *Ann Anat* **185**, 89–95.

Shilkrot LE, Srolovitz DJ (1998) Elastic analysis of finite stiffness bimaterial interfaces: application to dislocation-interface interactions. *J Appl Math* **46**, 3063–3075.

Smith KK, Hylander WL (1985) Strain gauge measurement of mesokinetic movement in the lizard *Varanus exanthematicus*. *J Exp Biol* **114**, 53–70.

Strait D, Wang Q, Dechow PC et al. (2005) Modeling elastic properties in finite element analysis: how much precision is needed to produce an accurate model? *Anat Rec A Discov Mol Cell Evol Biol* **283A**, 275–287.

Sun Z, Liu Z-J, Herring SW (2002) Movement of temporomandibular joint tissues during mastication and passive manipulation in miniature pigs. *Arch Oral Biol* **47**, 293–305.

Sun Z, Eugenia L, Herring SW (2004) Cranial sutures and bones: growth and fusion in relation to masticatory strain. *Anat Rec A Discov Mol Cell Evol Biol* **276A**, 150–161.

Thomopoulos S, Williams GR, Gimbel JA et al. (2003) Variation of biomechanical, structural, and compositional properties along the tendon to bone insertion. *J Orthop Res* **21**, 413–419.

Thomopoulos S, Marquez JP, Weinberger B et al. (2006) Collagen fiber orientation at the tendon to bone insertion and its influence on stress concentrations. *J Biomech* **39**, 1842–1851.

Wang Q, Dechow PC (2004) Variations in cortical material properties of baboon mandibles [abstract]. *Am J Phys Anthropol* **38**, 203.

Wang WJ, Crompton RH, Carey TS (2004) Comparison of inverse-dynamics musculo-skeletal models of AL 288-1Australopithecus afarensis and KNM-WT 15000 Homo ergaster to modern humans, with implications for the evolution of bipedalism. *J Hum Evol* **47**, 453–478.

Woo SL, Maynard J, Butler D (1987) *Ligament, Tendon, and Joint Capsule Insertions to Bone*. *Injury and Repair of the Musculoskeletal Soft Tissue*. Savannah: American Academy of Orthopaedic Surgeons.

Yamada H, Evans FG (1970) *Strength of Biological Materials*. Baltimore: Williams and Wilkens.

Zapata U, Metzger KA, Wang Q et al. (2010) Material properties of mandibular cortical bone in the American alligator, *Alligator mississippiensis*. *Bone* **46**, 860–867.